Japanese Journal of Applied Physics 51 (2012) 06FL09 **REGULAR PAPER**
DOI: 10.1143/JJAP.51.06FL09

Implementation of Complementary Metal–Oxide–Semiconductor Microelectromechanical Systems Lorentz Force Two Axis Angular Actuator

Chih-Ming Sun[1], Chung-Lin Wu[2], Chuanwei Wang[3], Chun-I Chang[1], Ming-Chuen Yip[3], and Weileun Fang[1,3]*

[1] *Institute of Nanoengineering and Microsystems, National Tsing Hua University, Hsinchu 300, Taiwan*
[2] *Center for Measurement Standards, Industrial Technology Research Institute, Hsinchu 300, Taiwan*
[3] *Department of Power Mechanical Engineering, National Tsing Hua University, Hsinchu 300, Taiwan*

Received November 29, 2011; accepted February 9, 2012; published online June 20, 2012

We present a novel dual-axis complementary metal–oxide–semiconductor (CMOS) microelectromechanical systems (MEMS) angular actuator driven by Lorentz force. The device has been successfully implemented using the Taiwan Semiconductor Manufacturing Company (TSMC) two-poly four-metal (2P4M) process. The current routing achieved with three metal layers enables independent driving for each axis. The measurement results show that the device has resonant frequencies of 1.36 and 2.26 kHz for the two axes.
© 2012 The Japan Society of Applied Physics

1. Introduction

The standard complementary metal–oxide–semiconductor (CMOS) process has been extensively applied to fabricate microelectromechanical systems (MEMS) devices. The applications of the standard CMOS process and special post-CMOS processes on MEMS have been reported.[1,2] The major advantage of the CMOS process is the monolithic integration of the IC and MEMS components. Hence, it is variously applied in the area of MEMS sensors.[3–5] In general, the process sequence, film materials and thickness, and layout rule have been strictly defined by the foundry-service CMOS process. Moreover, the thin-film residual stresses resulting from the processes frequently lead to unwanted deformation of the suspended CMOS MEMS structures. Thus, the design of MEMS components remains significantly limited by this standard process.

Electrostatic actuation is a very popular approach for driving microsystems because of its low power consumption. However, a high operating voltage is required. Other methods such as electrothermal and electromagnetic actuation, which can induce greater force and displacement, suffer from higher power consumption, long response time, and complicated fabrication, so the applications are restricted.[6–17] In recent years, Lorentz force actuators have become one of the attractive options for microsystem technology owing to their large force and displacement, fast response time, linear motion and acceptable power consumption.[18–22] Lorentz force excitation was also utilized in magnetic field detection. By using different electrical routings combined with structural design, the magnetometer for in-plane[23–27] and out-of-plane[28,29] magnetic field detection can be achieved. Furthermore, three-axis magnetometers for compass application have also been implemented.[30,31]

The CMOS MEMS actuators are far less available than their sensor counterpart to date. The CMOS MEMS actuators can be classified into two major categories: (1) in-plane and out-of-plane electrostatic comb-drive actuators[1–5] and (2) out-of-plane multilayer thermal actuators.[32,33] Although microactuators driven by a magnetic field have been extensively reported,[34–36] they are rarely seen for CMOS MEMS actuators. It is difficult to drive the CMOS MEMS device by means of magnetostatic force since the aluminum metal film is a paramagnetic material. Nevertheless, Lorentz force induced by magnetic field could be employed as the CMOS MEMS actuator. The Lorentz force MEMS actuator requires a metal layer for current routing. After applying a magnetic field to such a device, Lorentz force is induced by the current. The direction and magnitude of Lorentz force can be easily tuned by the input current. The application of Lorentz force to drive MEMS devices has been investigated.[34)]

In this study, we demonstrate the feasibility of driving the CMOS MEMS device using the magnetically induced Lorentz force, and successfully implement a CMOS MEMS moving stage with dual-axis angular displacements driven by Lorentz force. The device was fabricated using the existing foundry service, enabling further monolithic integration with control ICs.

2. Design Concept

The wire carrying a current of i inside a magnetic field of B will lead to Lorentz force F, which can be expressed as

$$F = iLB\sin\theta, \tag{1}$$

where L is the wire length and θ is the angle between the direction of magnetic field and current. Lorentz force F has been adopted to drive micromachined devices, such as the scanning mirror illustrated in Fig. 1. Thus, the magnitude and direction of driving force can be tuned by varying the current and the routing of wire.

In the present study, this characteristic has been further employed to drive a dual-axis CMOS scanning stage, as illustrated in Fig. 2. This stage consists of three major mechanical components, including torsional springs, a moving stage, and a supporting frame. The two pairs of torsional springs are designed to allow the moving stage and the supporting frame to rotate about two orthogonal axes. The design of the present stage is based on the two-poly four-metal (2P4M) processes. In this regard, the aforementioned mechanical structures are made of the four dielectric films (approximately 7 μm thick). Moreover, three of four metal (aluminum) layers are exploited to act as the conducting wires for current routing. The remaining metal layer is used as the etching mask.

In this study, we employed the Taiwan Semiconductor Manufacturing Company (TSMC) 0.35 2P4M CMOS

*E-mail address: fang@pme.nthu.edu.tw

 © 2012 The Japan Society of Applied Physics

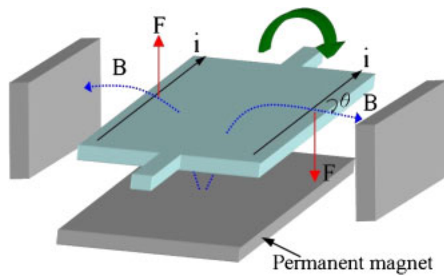

Fig. 1. (Color online) Concept of a scanning mirror driven by Lorentz force.

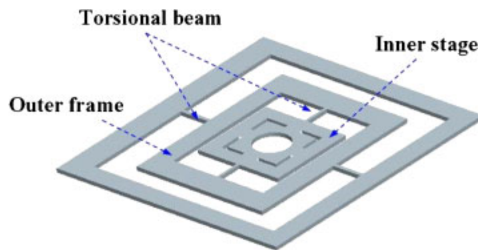

Fig. 2. (Color online) Schematic illustration of the dual-axis scanning stage.

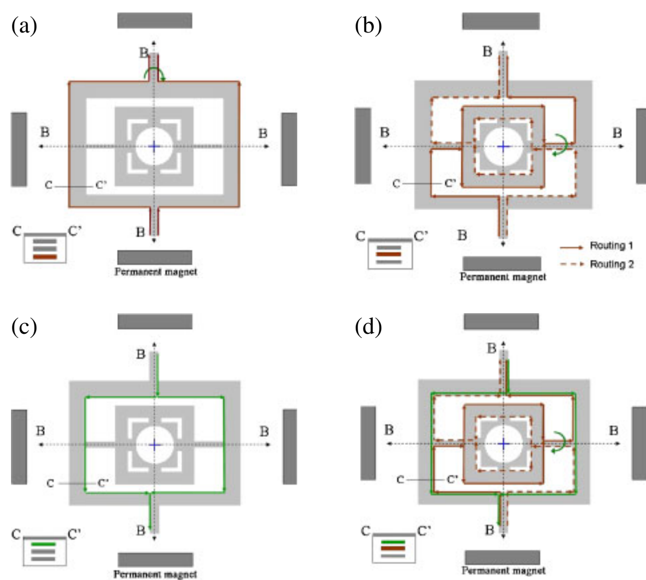

Fig. 3. (Color online) Schematic illustrations of the current routing for (a) outer frame driving, (b) inner stage driving, (c) outer frame current compensation, and (d) current of different directions for force compensation.

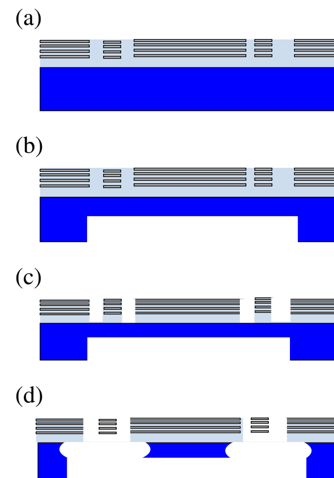

Fig. 4. (Color online) Process flow: (a) TSMC 0.35 μm 2P4M process, (b) ICP back etch to partially trim the substrate to 40 μm thickness, (c) RIE etching of silicon oxide, and (d) structure releasing by XeF_2 isotropic etching.[1)]

process to demonstrate the present device. The wire routing is designed to drive each axis of the stage independently. The routing of the first metal layer, illustrated in Fig. 3(a), is used to drive the outer supporting frame, whereas the routing of the second metal layer, in Fig. 3(b), is used to drive the inner moving stage. Owing to the magnetic field and current routing design, the Lorentz force will form a force couple on the stage, as illustrated in Fig. 1. Thus, the stage and the frame will experience pure angular motions by twisting movements. As indicated in Fig. 3(b), the current routing may induce the Lorentz force on the supporting frame while driving the moving stage. Thus, the outer frame will experience an unwanted angular motion. As shown in Fig. 3(c), we employed the third metal layer to act as the wire routing to compensate for the additional Lorentz force induced on the supporting frame. In the third metal layer, the wire is only distributed in the supporting frame. After applying the second and third layers with currents of the same magnitude but in the opposite direction, as indicated in Fig. 3(d), the induced Lorentz forces on the supporting frame (by the second and third metal layers) will cancel each other out. The concept of Lorentz force compensation has been applied on silicon-on-glass (SOG) scanner,[34)] however, several metal and dielectric insulation layers are required. Apparently, this approach is especially appropriate for the standard multi-metal-layers CMOS process.

3. CMOS Micromachining Post Process

The device after the TSMC 2P4M process is shown in Fig. 4(a). Figures 4(b)–4(d) show the post-CMOS processes. As shown in Fig. 4(b), the back of the silicon substrate was etched by deep reactive ion etching (DRIE) to partially trim the thickness of the substrate to 40 μm. After that, the reactive ion etching (RIE) was employed to remove the SiO_2 layer, as illustrated in Fig. 4(c). In this process, the top metal layer was used as the etching mask. Thus, the planar shape of the MEMS device was defined. Finally, the front of the silicon substrate was isotropically etched by XeF_2, as shown in Fig. 4(d). The CMOS structures were released from the substrate after the 40-μm-thick silicon layer was etched through by XeF_2.

Thus, the MEMS device was fully suspended and a thin-film spring was achieved as a flexible mechanical structure. In addition, a 40-μm-thick silicon layer was left on the back of the inner stage to enhance its flatness and stiffness. Figure 5(a) shows the scanning electron microscope (SEM) photograph of a typical fabricated device. The moving stage, supporting frame, and two pairs of torsional springs orthogonal to each other are clearly observed. The close-

© 2012 The Japan Society of Applied Physics

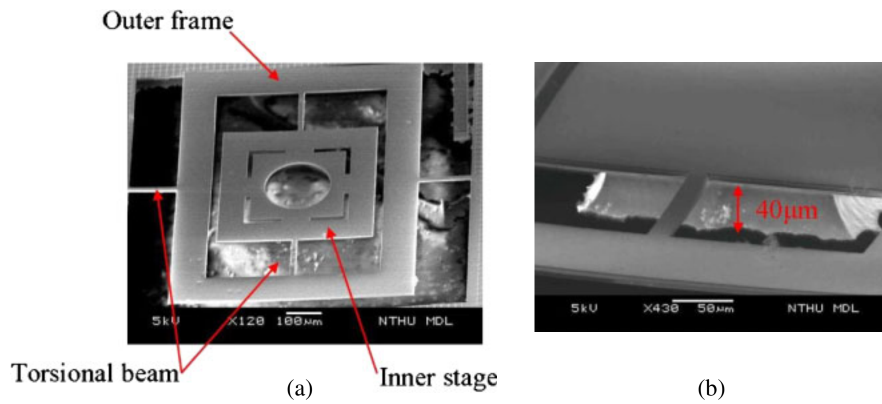

Fig. 5. (Color online) SEM images of (a) the fabricated scanning stage and (b) the close-up view of the back Si layer.

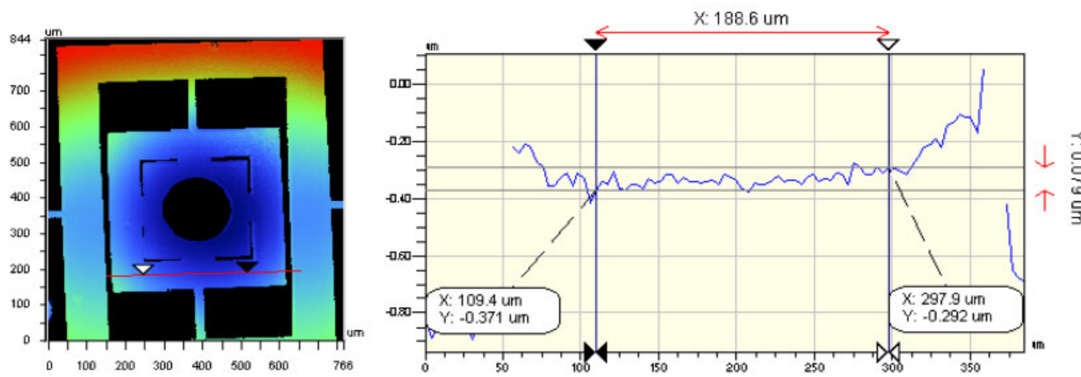

Fig. 6. (Color online) Measured radius of curvature of inner stage is 0.22 m.

up photograph in Fig. 5(b) shows the improved flatness and stiffness of the 40-μm-thick silicon layer.

4. Testing and Results

The radius of curvature (ROC) measured using the optical interferometer was 220 mm as shown in Fig. 6. However, the structure without the reinforced silicon layer was curved with a ROC of 4 mm. Thus, the flatness of the mirror has been improved by about 2 orders of magnitude. As a comparison, the 2-μm-thick poly-Si mirror has a ROC of $<$20 mm. Figure 7 shows the experimental setup for characterizing the performance of the CMOS dual stage. Figure 7(a) is a photograph of the sample holder and permanent magnets. In this case, a permanent magnet was placed under the MEMS device to generate a magnetic field towards the stage. Moreover, two pairs of permanent magnets surrounding the MEMS device were employed to redistribute the direction of the magnetic fields. This design is to ensure that the magnetic fields are distributed as indicated by the dashed lines in Fig. 3. Thus, according to eq. (1), the maximum Lorentz force on the device can be induced. The cross-sectional views of AA′ and CC′ in Fig. 7(b) show the specimen and the associated input current and magnetic fields. In summary, there are a total of five permanent magnets: one under the specimen and four placed around it. The gauss-meter measurement results in Fig. 7(c) indicate the distribution of the magnetic field provided by the five permanent magnets shown in Fig. 7(a). The measurements show an $8 \times 8 \times 3\,\text{mm}^3$ magnetic field. In this study, a chip of $3.68 \times 2.68 \times 0.6\,\text{mm}^3$ can be placed inside this magnetic field. The origin of the z-axis is the top surface of the permanent magnet under the MEMS device. In addition, the distance between the permanent magnet pair is 10 mm.

After applying the AC current to drive the device, the stage was under harmonic excitation. We tuned the driving frequency of the AC current, so as to find the frequency response of the dual stage. The dynamic response of the dual stage was measured using a commercial laser doppler vibrometer (LDV). Figure 8(a) shows the measured frequency response of the outer frame, and its resonant frequency is 1.36 kHz. Figure 8(b) shows the measured frequency response of the inner stage, and its resonant frequency is 2.26 kHz. Limited by the input current in the presented design (5 mA), the device has a small angular displacement of 0.24° at its resonant frequency. The dynamic responses in Fig. 8(b) indicate that the outer frame was also significantly excited while driving the inner stage. This was due to the fact that the routing of the inner stage had to pass through the outer frame, as illustrated in Fig. 3(c). We employed a compensation-current design on the outer frame to prevent it from excitation during the driving of the inner stage. The routings for compensation current and driving current were at metal 3 and metal 2

 © 2012 The Japan Society of Applied Physics

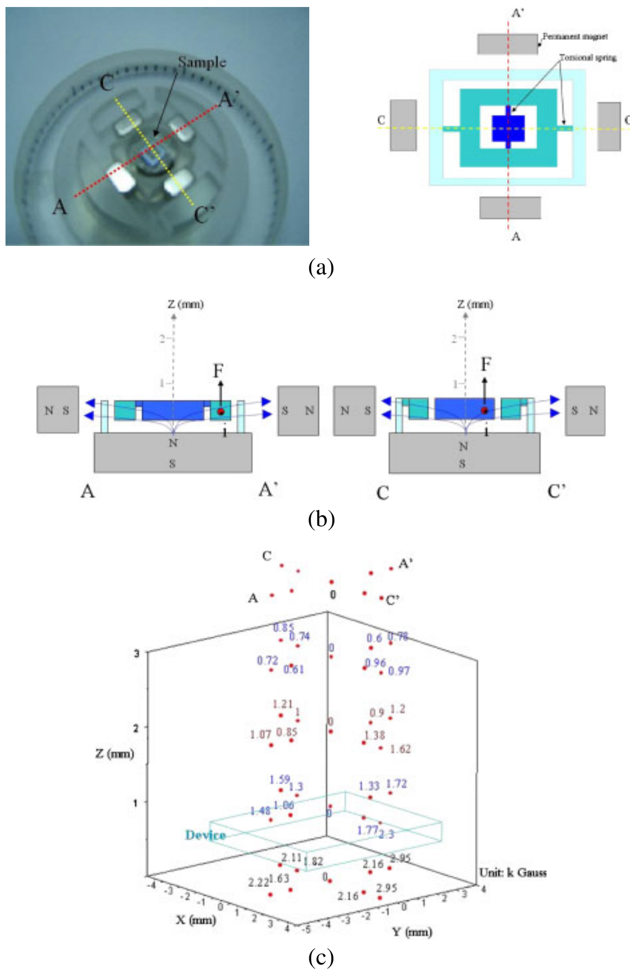

Fig. 7. (Color online) (a) Photograph and related schematic illustration of the test setup (b) the specimen and the associated input current and magnetic fields, and (c) the measured magnetic field distribution (kG).

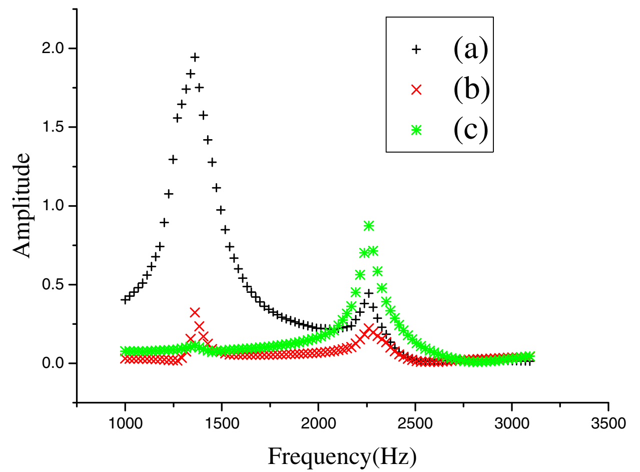

Fig. 8. (Color online) Frequency responses of the device at (a) outer frame, (b) inner stage, and (c) inner stage with current compensation. The resonant frequencies of the outer frame and inner stage are 1.36 and 2.26 kHz, respectively.

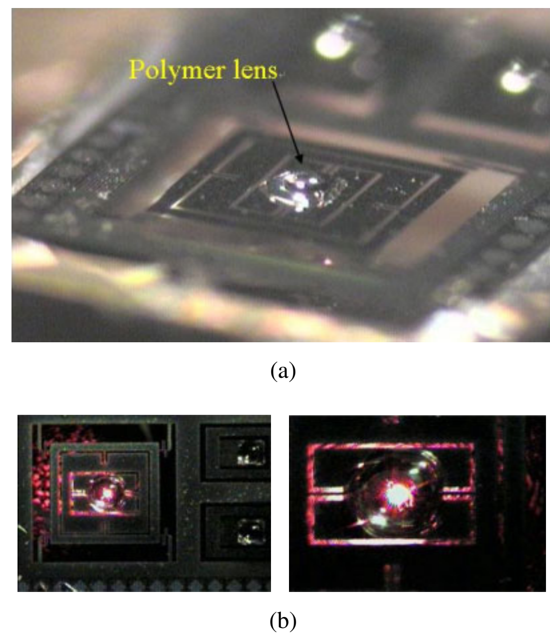

Fig. 9. (Color online) Photograph of the optical stage (a) with polymer lens, and (b) the laser beam passing through the polymer lens.

layers, respectively. Since the compensation and driving currents had the same magnitude but were in the opposite direction, the net Lorentz force on the outer frame became zero. The measurement results in Fig. 8(c) demonstrate that the dynamic response of the outer frame was successfully suppressed by the compensation current. The photographs in Fig. 9 further show the potential application of the presented moving stage driven by Lorentz force. As shown in Fig. 9(a), a polymer microlens is integrated with the stage by the dispensing process.[37,38] The laser beam can be modulated by the moving stage after passing through the microlens, as shown in Fig. 9(b).

5. Conclusions

We presented a novel CMOS MEMS scanning stage driven by Lorentz force. The feasibility of the scanning stage was demonstrated by the TSMC 2P4M process. The current routing achieved by adopting three metal layers enabled independent driving for each axis. The measurement results showed that the dual-axis stage was successfully driven by the present approach with resonant frequencies of 1.36 and 2.26 kHz for the two axes. We demonstrated the CMOS-MEMS Lorentz force actuator to drive the scanning mirror. The device has a small rotation angle (smaller than 0.95°) and displacement. In addition, we successfully applied the concept of current compensation to cancel out the unwanted Lorentz force during operation and showed that the multi-metal-layers CMOS process is more suitable for the present device. Thus, this could be a potential actuation mechanism for CMOS MEMS devices. Note the process nonuniformity resulting from the back DRIE silicon trimming and front XeF_2 silicon etching may have the following two effects on the actuator: (1) the thickness and shape of the 40-mm-thick silicon could be nonuniform and hence the mass and stiffness of the stage could also be nonuniform and (2) the boundary of the spring could be nonuniform after under-cutting XeF_2, and thus the spring stiffness of the actuator could be nonuniform. The proper control of the DRIE etching rate by the professional foundry can reduce the problem induced by the back DRIE. In addition, the adoption of front DRIE in the process before XeF_2 silicon

 © 2012 The Japan Society of Applied Physics

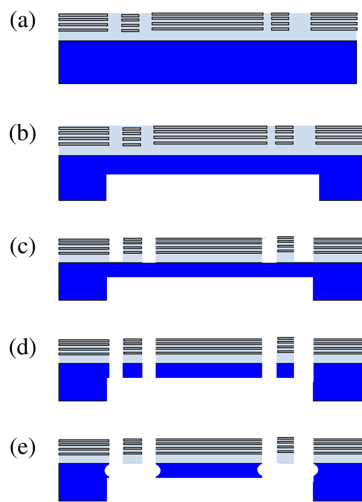

Fig. 10. (Color online) Revised process flow to reduce the problem of silicon undercutting by XeF_2.

etching, as illustrated in Fig. 10, is suggested. In this way, the XeF_2 silicon etching time and the boundary undercutting of the spring can be reduced.

Acknowledgements

This work was supported in part by the Ministry of Education, Taiwan, under grant 100N2049E1. The authors wish to thank the National Chip Implementation Center (CIC), Taiwan, for supporting this IC Manufacturing. The authors would also like to express their appreciation to the Center for Nano Science and Technology of National Tsing Hua University, and the Nano Facility Center of National Chiao Tung University for providing the fabrication facilities.

1) H. Xie, Y. Pan, and G. K. Fedder: J. Microelectron. Syst. **12** (2003) 450.
2) H. Xie, Y. Pan, and G. K. Fedder: Proc. ASME Int. Mechanical Engineering Congr. Expo., 2001, Vol. 3, p. 89.
3) H. Xie, G. K. Fedder, Z. Pan, and W. Frey: Proc. SM'03, 2003, p. 292.
4) H. Seidel, U. Fritsch, R. Gottinger, J. Schalk, J. Walter, and K. Ambaum: Proc. 8th Int. Conf. Solid-State Sensors and Actuators, and Eurosensors IX (Transducers '95), 1995, Vol. 1, p. 597.
5) D. J. Young and B. E. Boser: Proc. IEEE Integrated Circuit Conf., 1997, p. 5.
6) N. Asada, H. Matsuki, K. Minami, and M. Essashi: IEEE Trans. Magn. **30** (1994) 4647.
7) J. Hsieh and W. Fang: Sens. Actuators A **79** (2000) 64.
8) J. S. Ko, M. L. Lee, D. S. Lee, C. A. Choi, and Y. T. Kim: Appl. Phys. Lett. **81** (2002) 547.
9) W. C. Chen, C. C. Chu, J. Hsieh, and W. Fang: Sens. Actuators A **103** (2003) 48.
10) Y. J. Lai, C. Lee, C. Y. Wu, W. C. Chen, C. Chen, Y. S. Lin, W. Fang, and R. S. Huang: Jpn. J. Appl. Phys. **42** (2003) 4067.
11) H. K. Lee, K. S. Kim, and E. Yoon: IEEE Photonics Technol. Lett. **16** (2004) 2087.
12) W. Chen, C. Lee, C.-Y. Wu, and W. Fang: Sens. Actuators A **123–124** (2005) 563.
13) M. Wu and W. Fang: J. Micromech. Microeng. **16** (2006) 260.
14) S. Y. Lee, H. W. Tung, W. C. Chen, and W. Fang: IEEE Photonics Technol. Lett. **18** (2006) 2191.
15) A. Cao, P. Yuen, and L. Lin: J. Microelectromech. Syst. **16** (2007) 700.
16) M. Feldmann and S. Büttgenbach: IEEE Trans. Magn. **43** (2007) 3891.
17) D. A. Wang, H. T. Pham, and Y. H. Hsieh: Sens. Actuators A **149** (2009) 143.
18) L. O. S. Ferreira and S. Moehlecke: Sens. Actuators A **73** (1999) 252.
19) S. H. Ahn and Y. K. Kim: J. Micromech. Microeng. **14** (2004) 1455.
20) A. D. Yalcinkaya, H. Urey, D. Brown, T. Montague, and R. Sprague: J. Microelectromech. Syst. **15** (2006) 786.
21) T. Kobayashi and R. Maeda: Jpn. J. Appl. Phys. **46** (2007) 2781.
22) H. A. Yang, T. L. Tang, S.-T. Lee, and W. Fang: J. Microelectromech. Syst. **16** (2007) 511.
23) Zs. Kadar, A. Bossche, P. M. Sarro, and J. R. Mollinger: Sens. Actuators A **70** (1998) 225.
24) F. Keplinger, S. Kvasnica, A. Jachimowicz, F. Kohl, J. Steurer, and H. Hauser: Sens. Actuators A **110** (2004) 112.
25) V. Beroulle, Y. Bertrand, L. Latorre, and P. Nouet: Sens. Actuators A **103** (2003) 23.
26) R. Sunier, T. Vancura, Y. Li, K. K. Uwe, H. Baltes, and O. Brand: J. Microelectromech. Syst. **15** (2006) 1098.
27) A. L. Herrera-May, P. J. Garcia-Ramirez, L. A. Aguilera-Cortes, J. Martinez-Castillo, A. Carvajal, L. Garcia-Gonzalez, and E. Figueras-Costa: J. Micromech. Microeng. **19** (2009) 015016.
28) H. Emmerich and M. Schofthaler: IEEE Trans. Electron Devices **47** (2000) 972.
29) B. Bahreyni and C. Shafai: IEEE Sens. J. **7** (2007) 1326.
30) J. Kyynarainen, J. Saarilahti, H. Kattelus, A. Karkkainen, T. Meinander, A. Oja, P. Pekko, H. Seppa, M. Suhonen, H. Kuisma, S. Ruotsalainen, and M. Tilli: Sens. Actuators A **142** (2008) 561.
31) M. J. Thompson, M. Li, and D. A. Horsley: Proc. IEEE 24th Int. Conf. Micro Electro Mechanical Systems, 2011, p. 593.
32) H. Guckel, J. Klein, T. Christenson, K. Skrobis, M. Laudon, and E. G. Lovell: Tech. Dig. 5th Int. Conf. Solid-State Sensors and Actuators, 1992, p. 73.
33) A. Jain and H. Xie: IEEE Photonics Technol. Lett. **17** (2005) 1971.
34) S. H. Ahn and Y. K. Kim: J. Micromech. Microeng. **14** (2004) 1455.
35) H. A. Yang and W. Fang: Proc. IEEE MEMS Int. Conf., 2006, p. 774.
36) C. Lee: Sens. Actuators A **115** (2004) 581.
37) J. Hsieh, S. Y. Hsiao, C. F. Lai, and W. Fang: J. Micromech. Microeng. **17** (2007) 1703.
38) S. Y. Hsiao, C.-C. Lee, and W. Fang: J. Micromech. Microeng. **18** (2008) 085009.

© 2012 The Japan Society of Applied Physics